

# Small hydrocarbon molecules in cloud-forming Brown Dwarf and giant gas planet atmospheres

C. Bilger, P. Rimmer, Ch. Helling

*SUPA, School of Physics and Astronomy, University of St. Andrews, North Haugh, St. Andrews, Fife, United Kingdom, KY16 9SS*

Accepted 27 October 2021

## ABSTRACT

We study the abundances of complex carbon-bearing molecules in the oxygen-rich dust-forming atmospheres of Brown Dwarfs and giant gas planets. The inner atmospheric regions that form the inner boundary for thermochemical gas-phase models are investigated. Results from DRIFT-PHOENIX atmosphere simulations, which include the feedback of phase-non-equilibrium dust cloud formation on the atmospheric structure and the gas-phase abundances, are utilised. The resulting element depletion leads to a shift in the carbon-to-oxygen ratio such that several hydrocarbon molecules and cyanopolycyanopolyynene molecules can be present. An increase in surface gravity and/or a decrease in metallicity support the increase in the partial pressures of these species. CO, CO<sub>2</sub>, CH<sub>4</sub>, and HCN contain the largest fraction of carbon. In the upper atmosphere of low-metallicity objects, more carbon is contained in C<sub>4</sub>H than in CO, and also CH<sub>3</sub> and C<sub>2</sub>H<sub>2</sub> play an increasingly important role as carbon-sink. We determine chemical relaxation time-scales to evaluate if hydrocarbon molecules can be affected by transport-induced quenching. Our results suggest that a considerable amount of C<sub>2</sub>H<sub>6</sub> and C<sub>2</sub>H<sub>2</sub> could be expected in the upper atmospheres not only of giant gas planets, but also of Brown Dwarfs. However, the exact quenching height strongly depends on the data source used. These results will have an impact on future thermo-kinetic studies, as they change the inner boundary condition for those simulations.

## 1 INTRODUCTION

Brown Dwarfs and giant gas planets have atmospheres in which carbon is usually less abundant than oxygen. This may change if the planet forms in a disk with a carbon-rich dust-gas mixture (e.g. Fortney 2012), which seems unlikely for Brown Dwarfs that form from a molecular cloud by gravitational collapse. Both kind of objects, however, have atmospheres that are so cold that clouds form from the local atmospheric gas resulting in a depletion of elements, including oxygen and perhaps carbon. The formation of mineral clouds will individually deplete the heavy and less abundant elements like O, Mg, Si, Fe, Al, Ti (Helling & Woitke 2006; Witte et al. 2009) which makes the observational determination of the element abundances difficult. The depletion of oxygen is comparably moderate, but strong enough to shift the carbon-to-oxygen ratio (hereafter C/O ratio) from an initial solar value of  $\sim 0.5$  to  $\sim 0.7$ . The hypothesis of carbon-rich atmospheres in substellar objects is not new, and was inspired by observations of WASP-12b (Madhusudhan et al. 2011) and by questioning the standard planet composition (Gaidos 2000; Seager et al. 2007) earlier on. Our investigations are triggered by our finding (Sect. 4.1) that cloud formation alone causes a considerable shift in the local C/O ratio and the resulting question of how this changes the importance of carbon-bearing molecules in substellar atmospheres.

Independent of the model assumptions in cloud formation is that methane (CH<sub>4</sub>) becomes more abundant than carbon monoxide

(CO) at heights above roughly 1 bar in the dense atmospheres of cool Brown Dwarfs and giant gas planets (Helling et al. 2008, their Fig. 4). This is remarkable because the high binding energy of the CO-molecule causes the blocking of the carbon-chemistry in an oxygen-rich environment and vice versa. The reason is the high stability of the CO molecule due to its triple-binding between the C and the O atoms. CH<sub>4</sub> has four single covalent C-H bindings and as a result, is much more likely to react with other gas-phase species. Hence, CH<sub>4</sub> provides less rigid blocking of the carbon in an oxygen-rich environment. We will therefore investigate if this weakening of the carbon blocking might allow for the presence of even more complex carbon-binding molecules in the oxygen-rich atmospheres of Brown Dwarfs and giant gas planets, and this might be affected by vertical mixing.

Deviations from local chemical gas-phase equilibrium in the upper atmosphere are suggested to be caused by a rapid convective and/or diffusive up-mixing of warm gases from deeper atmospheric layers (e.g. Saumon et al. 2000, 2006, 2007; Leggett et al. 2007) in cold Brown Dwarfs (e.g. Gliese 229B, 570D) and giant gas planets. A similar process is discussed to affect the abundance determination in the solar system for Jupiter, Saturn, Uranus, and Neptune (Visscher & Moses 2011). Another possibility may be the impact of cosmic rays on the chemistry of the upper atmospheres of Brown Dwarfs.

Various groups (Zahnle et al. 2009a,b; Line et al. 2010; Moses et al. 2011; Venot et al. 2012) study the chemical kinetics under

arXiv:1307.2565v1 [astro-ph.SR] 9 Jul 2013

the influence of vertical mixing and photodissociation. All networks consider molecules formed of the elements H, C, O and N (Line et al. 2010 does not include nitrogen). The number of species and reaction differ between the chemical networks: Zahnle et al. (2009a) (used in Miller-Ricci Kempton et al. 2012) consider 58 species (561 kinetic reactions incl. 33 photo-chemical) and their network is accurate to  $C_2H_n$ . The species  $C_4H$  and  $C_4H_2$  are also included in their network. Line et al. (2010) consider 32 species (299 kinetic reactions incl. 41 photo-chemical), accurate to  $C_2H_2$ . Moses et al. (2011) consider 90 species ( $\sim 1600$  reactions), and incorporate hydrocarbons up to the size of benzene. Venot et al. (2012) consider 46 C/O species and 42 N-containing species ( $> 2000$  reactions incl. 34 photo-chemical reactions), accurate to  $C_2H_n$ . All these complex networks prescribe the atmospheric temperature-pressure profile and treat the eddy diffusion coefficient  $K_{\text{eddy}}$  as a parameter. The pressure-dependence of  $K_{\text{eddy}}$  is roughly determined by Line et al. (2010) and Moses et al. (2011). Moses et al. (2011) obtains  $K_{\text{eddy}}$  from the circulation models of Showman et al. (2009). Zahnle et al. (2009a) treat the gas temperature as isothermal, and Moses et al. (2011) and Venot et al. (2012) calculate  $(T, p)$  profiles from radiative transfer (Fortney et al. 2006, 2010) and hydrostatic equilibrium (Showman et al. 2009). None of these models has a comprehensive treatment of grain formation or the deposition of gas-phase species onto grains. The deviation from chemical equilibrium (or a steady state solution of the kinetic models) increases with increasing mixing efficiency which is a generally unknown parameter for planetary objects outside the solar system (Miller-Ricci Kempton et al. 2012). The deviations also tend to become more significant at lower pressures. The non-equilibrium steady-state and thermochemical equilibrium abundances agree to within an order of magnitude when  $p_{\text{gas}} \gtrsim 1 \text{ bar}$  ( $= 10^{-6} \text{ dyn/cm}^2$ ) (see Moses et al. 2011, their Fig. 8.) The inner boundary is an additional free parameter the impact of which is demonstrated by Venot et al. (2012, their Fig. 1). They also point out uncertainties in the  $NH_3$  and HCN abundances based on the use of different networks.

Our ansatz considers the collisional dominated inner part of an atmosphere where kinetic gas-phase modelling is not required, but which composes the inner boundary for kinetic gas-phase rate networks. In this part of the atmosphere, the local thermodynamic conditions are well constrained by atmosphere simulations that combine radiative transfer and cloud formation (Sect. 2.1 for more details). We consider the part of the atmosphere where the formation of dust clouds influences the local gas-phase chemistry, the local temperature and the density. The cloud formation causes a depletion of those elements which take part in the condensation process (e.g. Fe, Mg, O; Fig. 2) resulting in reduced abundances of respective molecules. Once the cloud particles have formed, they represent a very strong local opacity source absorbing in the optical and reemitting isotropically in the infrared. The consequence is a backwarming effect which causes a local increase of the gas temperature below the cloud layer (Fig. 1).

Given that collisional gas-phase processes dominate in the atmospheric part of interest, we apply a chemical equilibrium routine that allows us to provide first estimates of the abundances of carbon-bearing macro-molecules and small PAHs. This approach allows us to study the gas-phase abundances at the inner boundary of future kinetic considerations, and to look at species not presently included in most of the current networks (e.g.  $C_6H_6$ ). Furthermore, we show the influence of element abundances that are inhomogeneously depleted by the formation of dust clouds causing, for exam-

ple, a considerable shift in the local carbon-to-oxygen (C/O) ratio (Fig. 3). We discuss vertical mixing that transports gas to higher, hence, cooler atmospheric regions in comparison to the chemical relaxation timescale, and we assess the influence of uncertainties in rate coefficient data on the quenching height. The influence of cosmic rays on the upper atmosphere will be addressed in a forthcoming paper.

## 2 METHOD

We investigate the abundances of complex carbon-binding molecules in dust-forming, oxygen-rich atmospheres of Brown Dwarfs and giant gas planets by utilising chemical equilibrium calculations in combination with results from model atmosphere simulations (see Sect. 2.1). We are particularly interested in studying the effect of a changing C/O ratio on the remaining gas-phase chemistry as caused by element depletion during cloud formation.

### 2.1 Model atmosphere with cloud formation

We utilise results from the DRIFT-PHOENIX (Dehn 2007; Helling et al. 2008; Witte et al. 2009) grid of model atmosphere simulation which solves the classical 1D model atmosphere problem (radiative transfer, mixing length theory, hydrostatic equilibrium, gas-phase chemistry; PHOENIX; Hauschildt & Baron 1999) coupled to a cloud formation model (nucleation, surface growth and evaporation, gravitational settling, convective replenishment, element conservation; DRIFT; Woitke & Helling 2003, 2004; Helling & Woitke 2006). Each of the model atmospheres is determined by the effective temperature ( $T_{\text{eff}}$  [K]), the surface gravity ( $\log(g)$  with  $g$  in  $[\text{cm/s}^2]$ ), and a set of element abundances which have been chosen to be solar. These element abundances will be altered where dust forms as demonstrated in Fig. 2. The metallicity may be used as an additional parameter, and can be varied by homogeneously increase or decrease all elements to mimic a sub- or supersolar element abundance set. Additional input quantities are absorption coefficients for all atomic, molecular and dust opacity species considered. The cloud's opacity is calculated applying Mie and effective medium theory. For more details on Drift-Phoenix, refer to Witte et al. (2009).

Providing details on the dust clouds, such as height-dependent grain sizes, and the height-dependent composition of the mixed-material cloud particles, the model atmosphere code calculates atmospheric properties, like the local convective velocity, and the spectral energy distribution, etc. The relevant output quantities which we use for the present study are the temperature-pressure ( $T_{\text{gas}}$  [K],  $p_{\text{gas}}$  [ $\text{dyn/cm}^2$ ]) structure and the height-dependent element abundances  $\epsilon_i$  (Figs. 1, 2). The local temperature is the result of the radiative transfer solution and the local gas pressure of the hydrostatic equilibrium. The element abundances are the result of the element conservation equations that include the chance of elements by dust formation and evaporation.

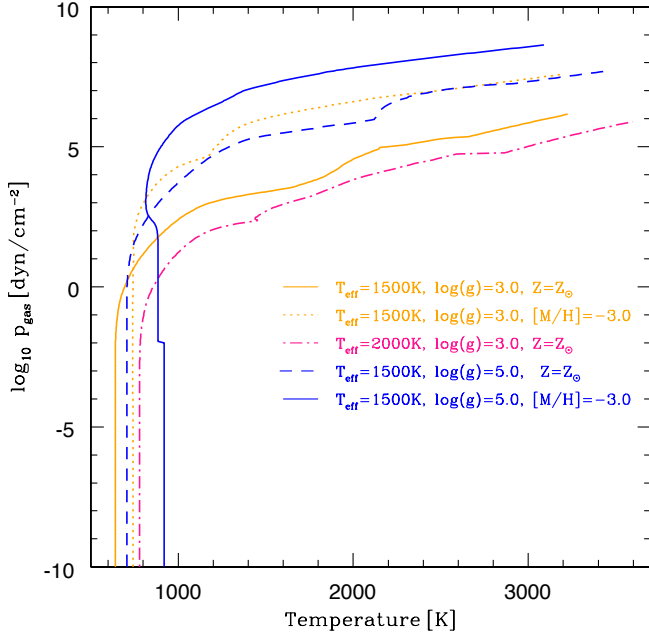


**Figure 1.** DRIFT-PHOENIX model atmospheric structures ( $T_{\text{gas}}$ ,  $p_{\text{gas}}$ ). The low-metallicity models ( $[M/H] = -3.0$ ) are always much denser than their solar counterpart ( $Z = Z_{\odot}$ ) for a given local temperature.

## 2.2 Chemical equilibrium calculation

In Local Thermodynamic Equilibrium (LTE), at a given temperature, gas pressure, and for a elemental composition, the chemical abundances depend on the thermodynamic properties of the species through their pressure equilibrium constants,  $K_p(T)$ . For an example dielemental molecule being formed from gaseous constituent atoms,  $K_p(T)$  is a function of temperature only, and is given by the law of mass action (e.g. Tsuji 1973; Gail & Sedlmayr 1986),

$$\ln K_p = \ln \frac{p(A)^a p(B)^b}{p(A_a B_b)} \quad (1)$$

where  $p(A_a B_b)$ ,  $p(A)$  and  $p(B)$  are the partial pressures of the molecule  $A_a B_b$  in LTE and constituent atoms A and B, respectively. The temperature dependence of  $K_p(T)$  can be fitted with a 4<sup>th</sup> order polynomial

$$\ln K_p = a_0 + a_1\theta + a_2\theta^2 + a_3\theta^3 + a_4\theta^4 \quad (2)$$

where  $\theta$  is the reciprocal temperature equal to  $5040/T$  (e.g. Tsuji 1973). Tabulated fitting parameters for the complex carbon-bearing molecules are from Cherchneff & Barker (1992). Each atom, molecule and ion is represented by the law of mass action, as well as satisfying element conservation and charge conservation. The partial pressure of the molecules, ions and atoms can then be converted into a number density,  $n_{A_a B_b}$ , by use of the ideal gas law

$$p(A_a B_b) = n_{A_a B_b} kT. \quad (3)$$

The equations are solved simultaneously for all gas-phase species.

The atmospheric profile of the local gas temperature, gas pressure, and element abundances are prescribed (DRIFT-PHOENIX model atmosphere results; Dehn (2007); Witte et al. (2009)) and the chemical equilibrium is evaluated for each atmospheric layer.

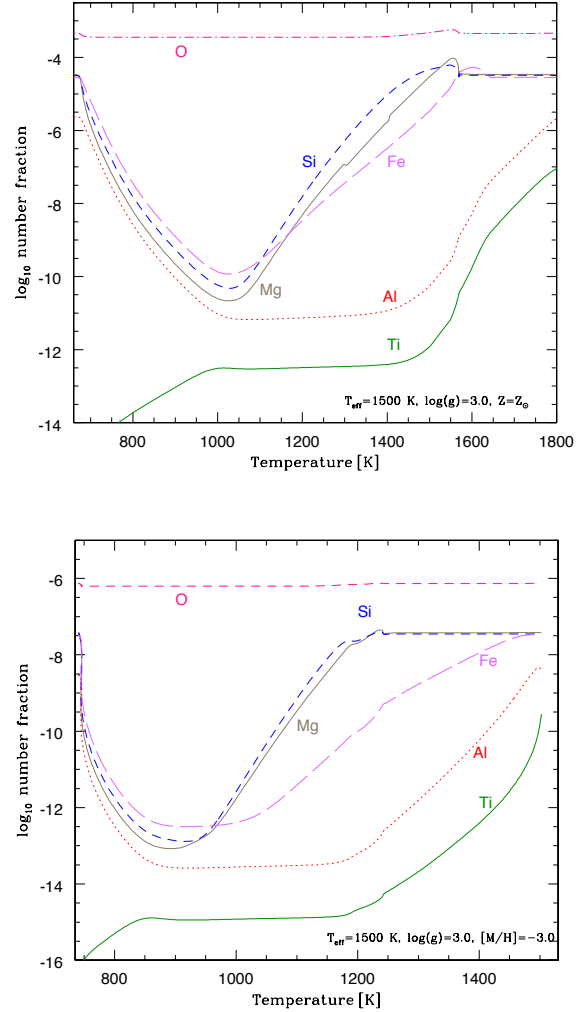


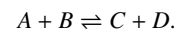
**Figure 2.** Gas-phase element abundances affected by dust formation in the atmosphere of a giant gas planet (DRIFT-PHOENIX atmosphere model:  $T_{\text{eff}} = 1500\text{K}$ ,  $\log(g) = 3$ ). *Top*: solar composition, *Bottom*: low-metallicity ( $[M/H] = -3.0$ ).

## 2.3 Chemical kinetic approach through quenching kinetics

In the deep atmospheric layers, at high temperatures and pressures, chemical equilibrium can prevail if reaction kinetics operate faster than convective mixing. This is when the time-scale for a species to reach thermochemical equilibrium,  $t_{\text{chem}}$ , is less than the timescale for atmospheric mixing,  $t_{\text{mix}}$  (Sect. 2.3.3 for more details). We consider vertical mixing as the *only* cause of non-equilibrium gas-phase chemistry here. We consider non-irradiated objects only, and hence, can neglect the effect of photo-chemistry for the time being.

### 2.3.1 Chemical relaxation time scale

Consider, for example, a gas-phase species, A, which is formed and destroyed solely by the gas-phase reaction:



The change in the number density of A,  $[A]$  [ $\text{cm}^{-3}$ ], is:

$$\left(\frac{d[A]}{dt}\right)_{p,T} = k_r(p, T)[C][D] - k_f(p, T)[A][B],$$

where  $k_f(p, T)$  is the forward reaction rate coefficient, and  $k_r(p, T)$  is the reverse reaction rate coefficient. Consider a given pressure and temperature,  $(p_0, T_0)$ , where  $(d[A]_0/dt)_{p_0, T_0} = 0$ . The densities  $[A]_0, [B]_0$ , etc. are the equilibrium densities for  $(p_0, T_0)$ . We now quickly<sup>1</sup> transport A in a large gas parcel to a new pressure and temperature,  $(p_1, T_1)$ , with new equilibrium densities,  $[A]_1, [B]_1$ , etc., where  $(d[A]_1/dt)_{p_1, T_1} = 0$ . If  $[A]_0 \gg [A]_1$ , then the time-scale,  $t_{\text{chem}}$ , for A to go from  $[A]_0 \rightarrow [A]_1$  can be expressed as (Prinn & Barshay 1977):

$$\frac{1}{t_{\text{chem}}} = \frac{1}{[A]_0} \left| \frac{d[A]_0}{dt} \right|_{p_1, T_1}$$

$$t_{\text{chem}} = \frac{[A]_0}{|k_f(p_1, T_1)[A]_0[B]_0 - k_r(p_1, T_1)[C]_0[D]_0|}.$$

The condition,  $[A]_0 \gg [A]_1$ , requires that:

$$k_f(p_1, T_1)[A]_0[B]_0 \gg k_r(p_1, T_1)[C]_0[D]_0.$$

If this were not the case, then the formation rate for A would be nearly equal or greater than the destruction rate for A, and at steady state, we would find  $[A]_0 \lesssim [A]_1$ , violating our required condition. In the case where  $[A]_0 \gg [A]_1$ , the reverse reaction rate can be neglected, and:

$$t_{\text{chem}} \approx \frac{1}{k_f(p_1, T_1)[B]_0}. \quad (4)$$

With this we consider that species A is destroyed by  $N$  reactions, each involving a species  $B_i$ , governed by a rate constants  $k_i$ . In this case, Eq. 4 is generalised as

$$t_{\text{chem}}(A) = \left( \sum_{i=0}^N k_i [B_i]_0 \right)^{-1}. \quad (5)$$

If a particular  $k_j [B_j]_0$  is much larger than any of the other  $k_i [B_i]_0$ , then Eq. 5 simplifies to

$$t_{\text{chem}}(A) \approx (k_j [B_j]_0)^{-1}. \quad (6)$$

The dominating destruction rate depends both on the rate coefficient,  $k_j$ , and on the number density of species B,  $[B_j]_0$  in the gas parcel. The chemical kinetic conversion timescale,  $t_{\text{chem}}(A)$  [s], for a given gas-phase species A, is the time for relaxation towards an equilibrium state. It is defined here as the time it takes for the number density,  $[A]$  [ $\text{cm}^{-3}$ ], to reach the equilibrium value. We describe our method for finding the dominant destruction reactions for select hydrocarbons in Section 3.2.

### 2.3.2 Mixing time scale

Large-scale convection is the transport of gases with the mean bulk flow. In contrast, diffusion refers to the transport of gases along a negative concentration gradient by the action of random motions. In the radiative zone, the vertical transport timescale by eddy diffusivity was suggested to be (e.g. Saumon et al. 2006; Moses et al.

2011).

$$t_{\text{mix, eddy}} = \frac{H_p(z)^2}{K_{\text{eddy}}}, \quad (7)$$

where  $H_p(z)$  is the local pressure scale height. The coefficient for eddy diffusion  $K_{\text{eddy}}$  was taken to be  $10^4$  and  $10^8 \text{ cm}^2 \text{ s}^{-1}$ , a set of reasonable values for substellar atmospheres (Saumon et al. 2006, 2007). A comparison with Zahnle et al. (2009a) and Moses et al. (2011) show that  $K_{\text{eddy}} = 10^8 \text{ cm}^2 \text{ s}^{-1}$  is on the low end of the values used in kinetic models. However, Miller-Ricci Kempton et al. (2012) studies mixing efficiencies down to  $K_{\text{eddy}} = 10^6 \text{ cm}^2 \text{ s}^{-1}$  for GJ1214b. Increasing the value of  $K_{\text{eddy}}$  increases the mixing which can yield larger departures from chemical equilibrium as shown by e.g. Zahnle et al. (2009a). The convective zone is situated in deeper atmospheric layers (the convective velocity is  $\neq 0$ ), however, Woitke & Helling (2004) developed the idea of convective overshooting. Driven by their momentum, the parcels of gas are able to ascend the atmosphere beyond the Schwarzschild boundary into the radiative zone. We compare the chemical kinetic conversion timescales ( $t_{\text{chem}}$ ; coloured lines in Figs. 12, 13) for the hydrocarbon species to the vertical convective overshooting timescales (thin black lines in Figs. 12, 13) of each atmosphere (see Woitke & Helling 2004, their Eq. 9) and to the eddy diffusion timescales (Eq. 7, thick black lines in Figs. 12, 13). The convective mixing involved in the Drift-Phoenix models does mainly impact chemistry-wise the cloud forming part of the atmosphere and decreases exponentially in the upper atmosphere. The diffusive mixing as applied in most of the complex chemical network evaluations sustains its efficiency throughout the whole atmosphere, moving slower in the inner atmosphere and faster in the higher atmosphere.

### 2.3.3 Quenching level

Deep in the atmosphere, the species in a gas parcel reach equilibrium with the surrounding gas faster than the time it takes for the gas parcel to reach the upper atmosphere. In the outer cooler atmosphere, however, energy barriers can become significant and vertical transport can dominate over chemical processes ( $t_{\text{chem}} > t_{\text{mix}}$ ). As a result, departures from chemical equilibrium can potentially be observed for some molecules (e.g.  $\text{CH}_4/\text{CO}$ , Saumon et al. 2006). The abundance of a molecular constituent may become “quenched” at a value called the “quench level”, when  $t_{\text{chem}} = t_{\text{mix}}$  (Prinn & Barshay 1977; Saumon et al. 2006; Visscher & Moses 2011; Moses et al. 2011). Above that level, at lower gas temperatures, the chemical reactions are frozen by vertical mixing, i.e. the forward chemical timescale is significantly slower than the gas-dynamic timescales involved. The intersection between the mixing timescale and the reaction timescale of a chemical species marks the point inside the atmosphere where the equilibrium number density of that species is “frozen in”, and from where on it remains roughly constant.

## 3 APPROACH

### 3.1 Equilibrium gas-phase chemistry calculation

A combination of 199 gas-phase molecules (including 33 complex carbon-bearing molecules), 16 atoms, and various ionic species

<sup>1</sup> fast enough that  $[A] \approx [A]_0$ ,  $[B] \approx [B]_0$ , etc.

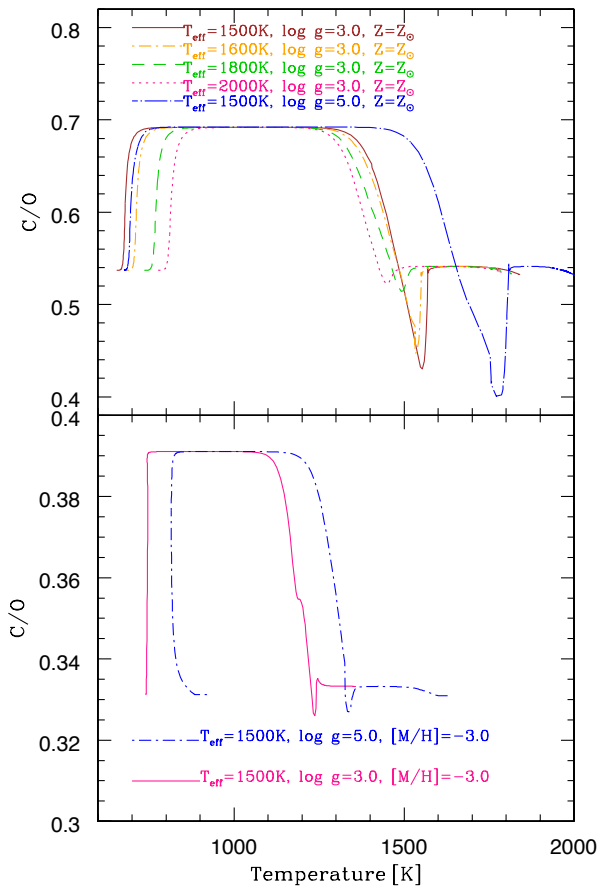


**Figure 3.** Carbon-to-oxygen ratios inside the dust cloud layer depending on  $T_{\text{eff}}$ ,  $\log(g)$  and metallicity  $[M/H]$ . The decrease below the initial value (top: solar, bottom:  $[M/H] = -3.0$ ) of the C/O ratio, is caused by the evaporation of the cloud particles.

were used under the assumption of LTE. This is an extension of the gas-phase chemistry routine used so far in our dust cloud formation according to Helling et al. (1996). The data for the large carbon-bearing molecules considered are taken from Cherchneff & Barker (1992) and they are grouped according to their structure as follows: large N-bearing species  $\text{HC}_x\text{N}$ , complex hydrocarbons  $\text{C}_n\text{H}_{2n\pm 2}$ ,  $\text{C}_2\text{H}_{2n}$ , CH-bearing radical  $\text{C}_x\text{H}$ ,  $\text{CH}_x$ , and  $\text{C}_x$ . The Grevesse et al. (2007) solar composition is used for calculating the gas-phase chemistry outside the metal depleted cloud layers and before cloud formation. No solid particles were included in the chemical equilibrium calculations but their presence influences the gas phase by the reduced element abundances due to cloud formation and the cloud opacity impact on the radiation field, both accounted for in the DRIFT-PHOENIX model simulations (Sect 2.1). We utilize DRIFT-PHOENIX model atmosphere ( $T_{\text{gas}}$ ,  $p_{\text{gas}}$ ,  $\epsilon_+$ ) structures as input for our chemistry calculations.

### 3.2 Reaction kinetics and rate determining steps

Various gas-phase rate networks are applied in the literature to study non-equilibrium gas-phase abundances in the upper low-pressure planetary atmospheres for irradiated objects (Zahnle et al. 2009a,b; Line et al. 2010; Moses et al. 2011; Venot et al. 2012; Miller-Ricci Kempton et al. 2012; Koppapu et al. 2012). Com-

plete chemical networks provide the ideal basis for determining quenching heights. The standard approach is to first model the atmosphere of a given object using a full rate network, and then to analyse the results of this network. Sensitivity analysis of networks can find rate-determining steps (Moses et al. 2011), and can even guide construction of a simplified network that includes only the dominant reactions (Carrasco et al. 2008). A comparison of the results for these networks is generally difficult because the rate networks differ in the number of rates. Therefore, the completeness of reaction paths, and often the reaction coefficient (e.g. Venot et al. 2012) and mixing parameter (e.g. Miller-Ricci Kempton et al. 2012) are not well constrained. A further challenge for rate network calculations is the choice of the inner boundary and the initial values for their kinetic equations.

Thus far, we have followed a chemical equilibrium approach to gain a first insight of how much element depletion by dust formation would support the existence of large carbon molecules in the collisional dominated part of the atmosphere which has well-determined thermodynamic properties (see Sect 2.1) compared to the diluted photo-chemically drive exosphere. To assess potential non-equilibrium effects on macroscopic carbon-binding molecules in the gas-phase due to quenching, we study time-scale for only  $\text{C}_2\text{H}_2$ ,  $\text{C}_2\text{H}_3$  and  $\text{C}_2\text{H}_6$ , for which we can provide the equilibrium values. We also investigate the possible effects of varying model atmosphere parameters (e.g. the surface gravity  $\log(g)$ ) in order to uncover potential differences between the extended atmosphere of a planet, and the much more compact atmosphere of Brown Dwarfs.

To investigate which molecule is driven out of equilibrium, one ideally uses an entire rate network because minor species might become unexpectedly important. However, it may also be possible to identify the dominant rate determining step which then would allow us an efficient assessment by using Eq. 6. This approach has been followed e.g. by Saumon et al. (2006) and was addressed also in Moses et al. (2011), and it has the advantage of flexibility. It further allows us to evaluate uncertainties in material quantities efficiently (Sect. 6.2). Carrasco et al. (2008) demonstrate how to produce a skeletal chemistry for Titan with the help of reference mass spectrum from INMS measurements of the Cassini Spacecraft. Their research is driven by the understanding that not all 700 reactions are needed to describe the Cassini observations. Their criterion is the reproduction of a certain reference observable within a certain uncertainty by a reduced set of reactions, starting from the full network.

We will explore the quenching heights of  $\text{C}_2\text{H}_2$ ,  $\text{C}_2\text{H}_3$ , and  $\text{C}_2\text{H}_6$  using a simplified method: We consider only the immediate destruction reactions for  $\text{C}_2\text{H}_2$ ,  $\text{C}_2\text{H}_3$ , and  $\text{C}_2\text{H}_6$  in order to calculate the value of  $t_{\text{chem}}$  using Eq. 6. We search for the dominant destruction reaction over the entire ( $T_{\text{gas}}$ ,  $p_{\text{gas}}$ ) profile. Three criteria guide our search for the dominant immediate destruction reaction. For a given reaction involving species A with abundance  $[A]_0$ , with a destruction reaction frequency  $\nu_f [\text{s}^{-1}]^2$ , and reverse reaction with a frequency  $\nu_r [\text{s}^{-1}]^2$ , there may be a range of ( $T_{\text{gas}}$ ,  $p_{\text{gas}}$ ) where:

<sup>2</sup> The reaction frequency is defined as  $\nu \equiv k_2[M]$  for combustion reactions,  $\nu \equiv k_2[B]$  for two-body reactions involving the species B, and  $\nu \equiv k_3[B][M]$  for three-body reactions involving B. In each case,  $k_2 [\text{cm}^3 \text{s}^{-1}]$  and  $k_3 [\text{cm}^6 \text{s}^{-1}]$  are measured rate coefficients and  $[M] [\text{cm}^{-3}]$  is the number density of the third body.

**Table 1.** Hydrocarbons' chemical reactions for kinetic calculations. The molecule M that appears in a few chemical reactions represents any third body.  $A$ ,  $n$  and  $E_a$  are used to calculate the rate coefficients  $k$  for *forward reactions*, although all the reactions are reversible.

Reaction	$A$ [ $\text{cm}^3 \text{s}^{-1}$ ]	$n$	$E_a$ [K]	$\Delta T$ [K]	References
$\text{C}_2\text{H}_2 + \text{H} \xrightarrow{\text{M}} \text{C}_2\text{H}_3$	$3.3 \times 10^{-30}{}^a$	0.0	740	200 – 400	Baulch et al. (1992)
$b$	$1.4 \times 10^{-11}$	0.0	1220	300 – 2000	Baulch et al. (1992)
$\text{C}_2\text{H}_2 \xrightarrow{\text{M}} \text{Products}$	$1.1 \times 10^{-10}$	0.0	20880	1500 – 3500	Durán et al. (1989)
$b$	$1.0 \times 10^8{}^c$	0.0	20400	700 – 2500	Klotz et al. (1980)
$\text{C}_2\text{H}_3 + \text{H}_2 \rightarrow \text{C}_2\text{H}_4 + \text{H}$	$3.4 \times 10^{-14}$	2.6	2525	300 – 2500	Knyazev et al. (1996)
$\text{C}_2\text{H}_6 \xrightarrow{\text{M}} \text{CH}_3 + \text{CH}_3$	$1.9 \times 10^9$	-13	51000	700 – 1924	Oehlschlaeger et al. (2005)
$b$	$1.7 \times 10^{26}{}^c$	-9.7	53900	700 – 1924	Oehlschlaeger et al. (2005)

<sup>a</sup> Units of [ $\text{cm}^6 \text{s}^{-1}$ ]<sup>b</sup> This rate coefficient is for the reaction above in the high pressure limit. This can be combined with the above rate coefficient as described in Visscher & Moses (2011).<sup>c</sup> Units of [ $\text{s}^{-1}$ ]

- (i) The reaction is reversible.
- (ii)  $v_f \gg v_r$ .
- (iii)  $v_f$  is much greater than the measured destruction frequency for other destruction reactions.

If these three criteria are met for a range of our ( $T_{\text{gas}}$ ,  $p_{\text{gas}}$ ) profile, then we consider that reaction to be the dominant destruction reaction for that range. We applied these three criteria in the case of  $\text{C}_2\text{H}_2$ ,  $\text{C}_2\text{H}_3$ , and  $\text{C}_2\text{H}_6$ . We obtained the rate coefficients for the destruction reactions by searching the NIST Kinetics Database (<http://kinetics.nist.gov/>), the UMIST Database for Astrochemistry, the reaction list from Moses et al. (2005, [www.lpi.usra.edu/science/moses/reaction\\_list.pdf](http://www.lpi.usra.edu/science/moses/reaction_list.pdf)) and from (Venot et al. 2012), available on the KIDA database (Wakelam et al. 2012, <http://kida.obs.u-bordeaux1.fr>). Reverse reactions were obtained from NIST, where available. When NIST did not list the reverse reactions, the rate coefficients were calculated from the assumption of microscopic reversibility, employing the method outlined in Visscher & Moses (2011). For each of the dozens of reactions, we calculated the destruction reaction frequency, and the reverse (formation) reaction frequency. The reactions that met all three criteria above are listed along with their rate coefficients in Table 1.

The rate coefficients for the dominant destruction reactions,  $k$ , are given by the Arrhenius equation:

$$k = A \left( \frac{T}{298 \text{ K}} \right)^n e^{-E_a/T}. \quad (8)$$

Where  $A$ ,  $n$  and  $E_a$  are parameters taken from the sources mentioned above. Units of  $k$  are  $\text{s}^{-1}$ ,  $\text{cm}^3 \text{s}^{-1}$  and  $\text{cm}^6 \text{s}^{-1}$  for first-, second- and third-order reactions, respectively. Table 1 contains the dominant destruction reactions for  $\text{C}_2\text{H}_2$ ,  $\text{C}_2\text{H}_3$  and  $\text{C}_2\text{H}_6$ . Multiple destruction rates are listed because different destruction reactions dominate at different pressures.

The listed reactions may differ for different atmospheres of different objects or for an atmosphere with different element abundances, e.g. for a  $\text{N}_2$  dominated atmosphere which is the case also for full rate networks. This method cannot account for the nonlinear nature of the full kinetics treatment, but no current chemical kinetics model is able to account for the deposition of gas-phase

species onto dust grains as done in the DRIFT-PHOENIX atmosphere models used here.

The purpose of our approach is to constrain quenching heights for select small hydrocarbons to indicate potentially arising non-equilibrium effects starting from our equilibrium abundances of carbon-binding macro-molecules. Since our intent is not to incorporate any non-equilibrium processes other than atmospheric mixing, this simplistic time-scale comparison seems capable of determining whether a given species is quenched, and what range of heights at which it is likely to be quenched. Although solving the series of nonlinear coupled differential equations describing the full chemical kinetics is in general the most complete approach, in this case it would risk amplifying uncertainties (Wakelam et al. 2005) by using large computing resources. A detailed discussion of the reasons for these uncertainties and their effect on our investigation is presented in Sec. 5.

A considerable uncertainty is hidden in the designation of the reactions in Table 1 due to uncertainties in laboratory and theoretical investigations. Errors in the treatment of reaction kinetics (incorrect assumptions about the rate-determining step or rate coefficient) are common, and may lead to uncertainties in the conclusions regarding disequilibrium abundances. This has been demonstrated by Venot et al. (2012) for the competing abundances of  $\text{NH}_3$  and  $\text{HCN}$ . This problem is known in the wider astronomical community and has led to comparative studies of PDR chemical networks (e.g. Röllig et al 2007; PDR - photo-dissociation regions).

Our list of reactions in Table 1 is constructed based on the best available measured and calculated rate coefficients. As this knowledge improves, the list of reactions might change, and so would the quenching height, independent of the approach chosen. Similar risks are present when analyzing the chemistry using a comprehensive chemical network. To our knowledge, the reactions in Table 1 are the most efficient destruction routes for the species we consider.

## 4 CHEMICAL EQUILIBRIUM RESULTS

In what follows, we present our results of the composition of the gas of the deeper atmospheric layers, i.e. below the uppermost at-

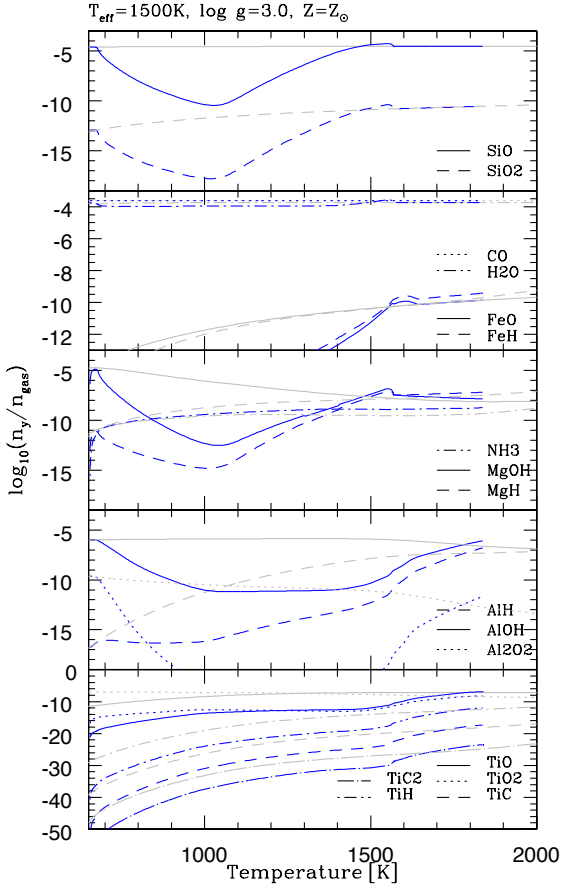


**Figure 4.** The impact of dust-depleted element abundances on the gas-phase composition. Only molecules involved in dust formation and those typically appearing in a dense, oxygen-rich atmosphere are shown: grey – no element depletion (solar abundances), blue – dust depleted element abundances. We utilise a giant gas planet DRIFT-PHOENIX model atmosphere ( $T_{\text{eff}}=1500\text{K}$ ,  $\log(g)=3.0$ , initial solar).

atmosphere which could be affected by photochemistry. We are interested in how cloud formation may indirectly impact the occurrence or the increase of the number density of complex carbon molecules in oxygen-rich environments. Such an indirect influence results from an inhomogeneous depletion of elements due to the formation of cloud particles, and from the feedback on the local temperature-pressure structure due to the large opacity of a dust cloud. We study the effect of the atmosphere model parameter ( $T_{\text{eff}}$ ,  $\log(g)$ , metallicity), and investigate a case for an artificially increased carbon over oxygen abundance.

We present the calculations of the gas-phase abundances for a given atmospheric structure. The local temperature, pressure and element abundances are a result of the DRIFT-PHOENIX atmospheric simulations (see Sect. 2.1). In Sect. 4.1 the local gas-phase element abundances are discussed with respect to the element depletion due to cloud formation. These element abundances are input quantities for our chemical equilibrium routine. Their impact on the gas-phase compositions is demonstrated in Sect. 4.2 for an example of a giant-gas planet model atmosphere ( $T_{\text{eff}} = 1500\text{K}$ ,  $\log(g)=3.0$ , initial solar element abundances). Section 4.3 shows which carbon-binding macro-molecules, small PAHs and HCN molecules could be expected in chemical equilibrium in the dense, cloud forming part of a Brown Dwarf or giant gas planet’s atmosphere. Both dif-

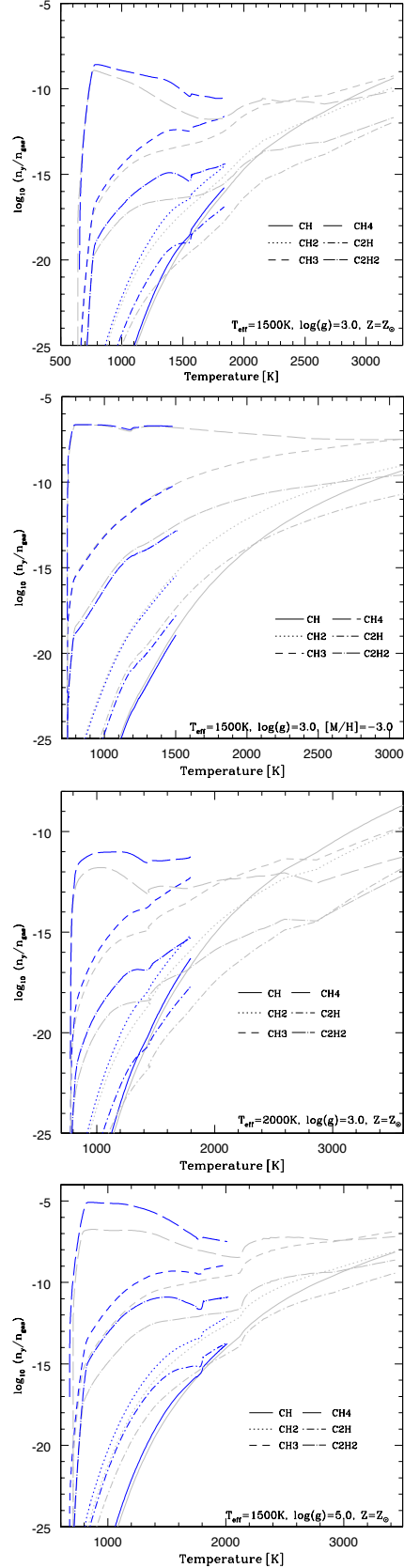


**Figure 5.** Gas composition for [C,H]-bearing gas-phase molecules: grey – no element depletion (solar abundances), blue – dust depleted element abundances. We utilise a giant gas planet DRIFT-PHOENIX model atmosphere ( $T_{\text{eff}}=1500\text{K}$ ,  $\log(g)=3.0$ , initial solar).

fer by their gravitational surface acceleration ( $\log(g)$ ), which causes the giant gas planet to have a much larger pressure scale height in the atmosphere, hence, to be less dense than a Brown Dwarf atmosphere. Section 4.5 tests how our results change if the C/O ratio is increased to larger than one.

#### 4.1 Element abundances

The cloud formation as part of the DRIFT-PHOENIX atmosphere simulations affects the metal elements O, Ti, Mg, Si, Fe, Al which are depleted by the amount needed to form the cloud particles. This results a metal-depleted gas-phase. This becomes apparent in Fig. 2: the metal elements decrease as dust forms. Deeper inside the atmosphere, after evaporation of the dust grains, the metal elements are released back into the gas-phase. The relative depletion is independent on the initial element abundances as a comparison between the upper (solar) and the lower (subsolar) panel of Fig. 2 shows.

The depletion of the oxygen causes the carbon-to-oxygen ratio to increase as relatively more carbon is available than without dust formation. Figure 3 demonstrates further that the change in C/O from the solar value to  $\sim 0.7$  is independent of the stellar parameters  $T_{\text{eff}}$  and  $\log(g)$ . Only the atmospheric gas temperature range concerned becomes wider with increasing gravity, hence for Brown Dwarfs, slightly more oxygen is available at the cloud base compared to a gas giant's atmosphere.

The drop below the initial value (solar or  $[M/H] = -3.0$ ) of the C/O ratio, is caused by a rise in the number fraction of oxygen at the cloud base following the gravitational settling and complete evaporation of dust particles containing oxygen.

#### 4.2 Reference calculations

The elemental abundances determine how much of a given element is available to form molecules or ions. We have chosen one example model to demonstrate how different the molecular abundances are for a dust-depleted (blue) and a non-depleted (grey) element composition for an oxygen-rich planetary atmosphere of  $T_{\text{eff}} = 1500\text{K}$ ,  $\log(g)=3.0$  and (initial) solar metallicity (Figure 4). Oxygen-bearing, dust forming molecules can be considerably less abundant inside the cloud layers which coincides with the deviation of the elements from their initial values, because the dust formation processes consumes the local elements. This is shown in Fig. 2 where the cloud layer spans a temperature range from  $T_{\text{gas}} = 100 \dots \sim 1600\text{K}$  for the low-metallicity giant gas planet atmosphere (bottom panel).

As the metal elements are depleted by dust formation, they become unavailable to the formation of typical oxygen-rich gas-phase molecules (e.g. SiO, FeO, MgOH). The Ti-bearing gases are the least abundant; the Fe-, Al-, Si-, and Mg-bearing gases have concentrations  $\log(n_y/n_{\text{gas}}) \approx 10^{-5} \dots \approx 10^{-15}$ , hence they decrease by orders of magnitude inside the cloud region. We observe further that molecules such as, e.g.  $\text{NH}_3$ , which are not directly involved in dust formation can change their abundance if dust forms. This is largely due to the effect of dust formation on the gas-phase metallicity, and its effect on the atmospheric temperature structure.

Figure 4 demonstrates the major reservoir for oxygen in sub-

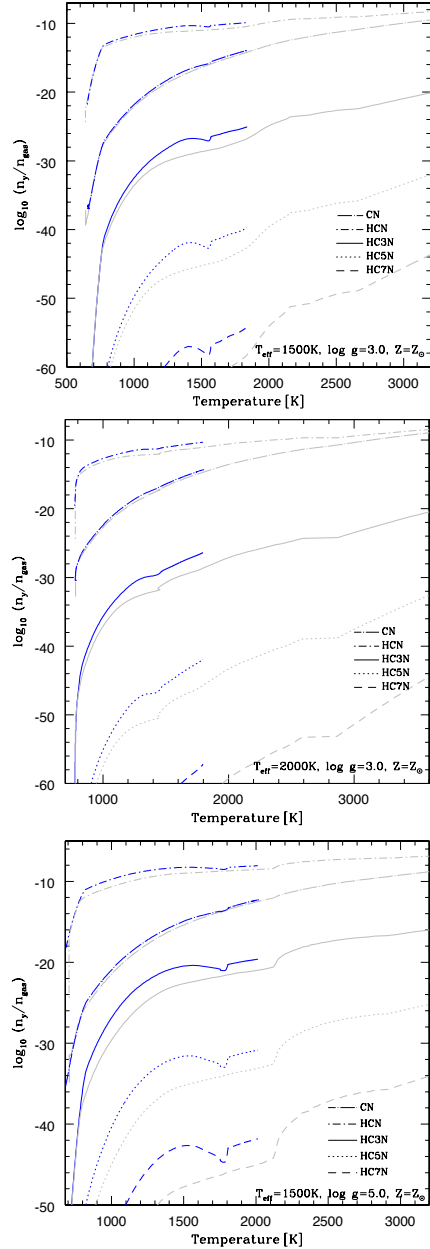


**Figure 7.** Molecular number densities,  $\frac{n_y}{n_{\text{gas}}}$ , of typical [C,N]-bearing gas-phase molecules for a giant gas planet and a Brown Dwarf based on DRIFT-PHOENIX model atmospheres. The  $\text{HC}_x\text{N}$  are generally low abundant and not much changes amongst the models investigated in this paper.

stellar oxygen-rich atmospheres are gaseous  $\text{H}_2\text{O}$  and CO.  $\text{CH}_4$  is the most abundant hydrocarbon (Fig. 5). Its concentration ( $\approx 10^{-5}$ – $10^{-10}$ ) is comparable to the concentration of the typical oxygen-binding molecular species encountered in substellar atmospheres. We refer for a more complete plots regarding to oxygen-rich gas-phase abundances to e.g. Lodders & Fegley (2002).

#### 4.3 Hydrocarbons & PAH's

Carbon and hydrocarbon macro-molecules are not included in the dust cloud formation considered in the DRIFT-PHOENIX model at-

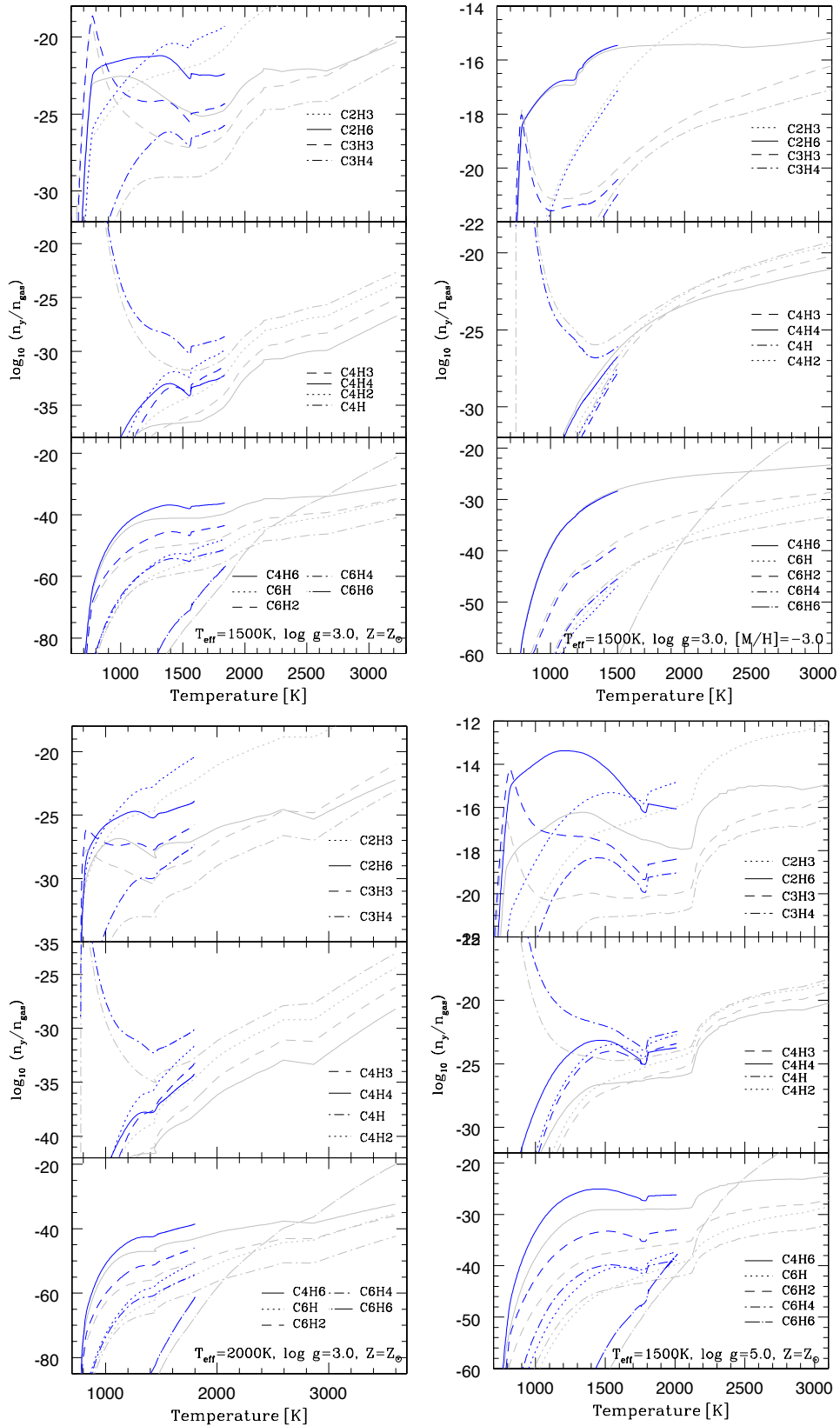


Figure 6. Same as Figure 5 for small hydrocarbon molecules.

mospheres, nor in any of the other model atmosphere simulations for substellar objects. But dust formation has a strong impact on the oxygen abundance. Because of the large abundance of oxygen compared to iron, magnesium etc, the change seems small at a first glance, but the resulting C/O ratio is considerable (Sect. 4.1). The question is: how many carbon-bearing macromolecules would we expect in the collisionally dominated chemistry of a denser atmospheric environment, and how would this change if an oxygen-depleting process like cloud formation occurred? Our calculations will serve as an inner boundary for more complex, kinetic models that are not yet able to resolve all possible reaction paths, and that address the outer atmospheric regions only (Zahnle et al. 2009, Line et al. 2010, Moses et al. 2011, Venot et al. 2012).

We find that inside the cloud layer where oxygen is depleted, the carbon-bearing molecules, including the CN-complex, are more abundant than outside the cloud layer. For example,  $C_2H_6$  increases by 3 orders of magnitude in concentration,  $C_4H_4$  by 4 orders of magnitude and  $CH_4$  by 1.5 order of magnitude (Figs. 5, 6;  $T_{\text{eff}}=1500\text{K}$ ,  $\log(g)=3.0$  and solar). CO, on the other hand, does not vary visibly (Fig. 4). The effect is smaller for the CN-molecules (Fig. 7).

All number densities rise, with the exception of  $C_4H$ , with local gas temperature as the gas density increase inside the atmosphere. A higher density allows more molecules to form as the atmospheric number density increases. The smaller member of the hydrocarbon groups is always the most abundant. However,  $C_6H_6$  (the first *aromatic ring*, or PAH) becomes one of the most abundant hydrocarbons in the deeper atmospheric layers. Its number density is comparable to the one of TiO or to hydrocarbons bearing 2 or 3 carbon atoms (Fig. 4). The results may appear surprising, but the atmospheric environments that we investigate here are considerably more dense than for example the atmosphere of an AGB star by which the study of carbon-molecules was inspired.

The PAHs, other than  $C_6H_6$ , do not form in significant quantities. The little ‘‘dip’’ observed in each curve is due to the drop of the C/O ratio at  $\sim 1550\text{K}$  (model dependent). It is attributed to a sudden small rise in the number fraction of oxygen upon elemental oxygen replenishment of the cloud base following the gravitational settling and complete evaporation of dust particles containing oxygen.

**Varying  $T_{\text{eff}}$ ,  $\log(g)$  and  $[M/H]$ :** We study the influence of  $T_{\text{eff}}$ ,  $\log(g)$  and  $[M/H]$  on the molecular concentrations. An increase of the effective temperature to  $T_{\text{eff}} = 2000\text{K}$  causes decreasing number densities of the macro-molecules considered here. This is a consequence of a lower gas pressure for a given temperature in the atmosphere. It must be noted that all carbon-bearing molecular abundances remain greater inside the cloud layers than outside, even for increasing  $T_{\text{eff}}$ .

Carbon-bearing species are able to form in higher abundances inside the cloud layers for an increasing surface gravity, i.e. inside Brown Dwarfs’ atmospheres. This is a consequence of the higher gas pressure throughout their atmosphere compared to a gas giant’s atmosphere. Increasing the surface gravity increases the partial pressures of the gas-phase molecules and hence their number densities. The pronounced jump in the number densities at  $\sim 2150\text{K}$  coincides with the  $(T, p)$ -structure of the model. It is a feedback that results from dust formation causing a backwarming effect. In spite of this increase in gas pressure, hydrocarbons with 6 or 4 car-

bon atoms are still very rare ( $< 10^{-20}$  in concentration). Benzene is again an exception in the deeper atmospheric layers, where it reaches a concentration of  $10^{-9}$  for the very low-metallicity cases, which is comparable to the oxygen-bearing molecules’ concentration shown in Fig. 4. Note, that low-metallicity atmospheres are considerably denser than solar metallicity atmospheres as demonstrated by Fig. 1.

The metallicity is another parameter that determines the structure of a (model) atmosphere, but it is not very well constrained as our results in Sect. 4.1 suggest. The metallicity parameter is often introduced because detailed knowledge of individually varying element abundances is only very scarcely available. Works by Burgasser and co-workers show that metallicity needs to be considered as a parameter also for Brown Dwarfs and giant gas planets.

By decreasing the metallicity,  $[M/H]$ , atomic hydrogen becomes even more abundant relative to heavier elements. The concentrations of the different H-bearing species throughout the atmosphere increase compared to the solar composition case. Molecules with a higher number of H-atoms (e.g.  $CH_4$  and  $C_2H_6$ ) remain in higher concentration inside the cloud layer, although by a much smaller fraction than in the solar-metallicity models studied. This small surplus in the concentration of some hydrocarbons leads to a lowering of the abundances of the other carbon-bearing molecules and compensates for the disappearance of hydrogen-saturated carbon-containing species.

#### 4.4 The carbon fraction locked up in carbonaceous molecules

In substellar atmospheres, most of the hydrogen is locked in  $H_2$ , and most of the carbon is in CO or  $CH_4$ . In this section, we calculate the carbon fraction locked in some hydrocarbon and cyanopolyne molecules to test for the presence of alternative dominant equilibrium forms of carbon under the temperature and pressure conditions considered in this work following the work by Helling et al. (1996). To calculate the fraction of carbon, by mass, locked into each carbon-bearing molecule, we used

$$F_y = \frac{N_C \times m_H \times [y]}{\rho_C} \quad (9)$$

where  $N_C$  is the number of carbon atoms in molecule  $y$ ,  $m_H$  is the mass in grams of a carbon atom,  $[y]$  is the number density of molecule  $y$  [ $\text{cm}^{-3}$ ] and  $\rho_C$  is the total carbon mass density [ $\text{g cm}^{-3}$ ] in the gas-phase.

Figure 8 depicts the fraction  $F_y$  of carbon atoms bound in species  $y$  along the temperature profile of the cloud layer of a giant gas planet with  $T_{\text{eff}}=1500\text{K}$ ,  $\log(g)=3.0$  and solar element abundances. It is remarkable that, in the outer layers,  $C_4H$  traps most of the available atomic carbon, before dropping exponentially. From  $500\text{K}$  onwards, CO,  $CO_2$  and  $CH_4$  establish themselves as the dominant carbon-bearing molecules throughout the cloud layer.

**Influence of  $T_{\text{eff}}$ ,  $\log(g)$  and  $[M/H]$ :** When the effective temperature is increased to  $2000\text{K}$  (lower left panel in Fig. 8),  $F_y$  generally diminishes since the molecular number densities have decreased.  $F_{C_4H}$  substantially decreases and substitutes CO and  $CO_2$  as the main carbon-bearing species in the very outer layers of the atmosphere. In a Brown Dwarf ( $\log(g)=5.0$ ),  $CH_4$  is substituted as a more important carbon-bearing molecule than  $CO_2$ .

In a low metallicity environment ( $[M/H]=-3.0$ ), CO and  $CO_2$  are

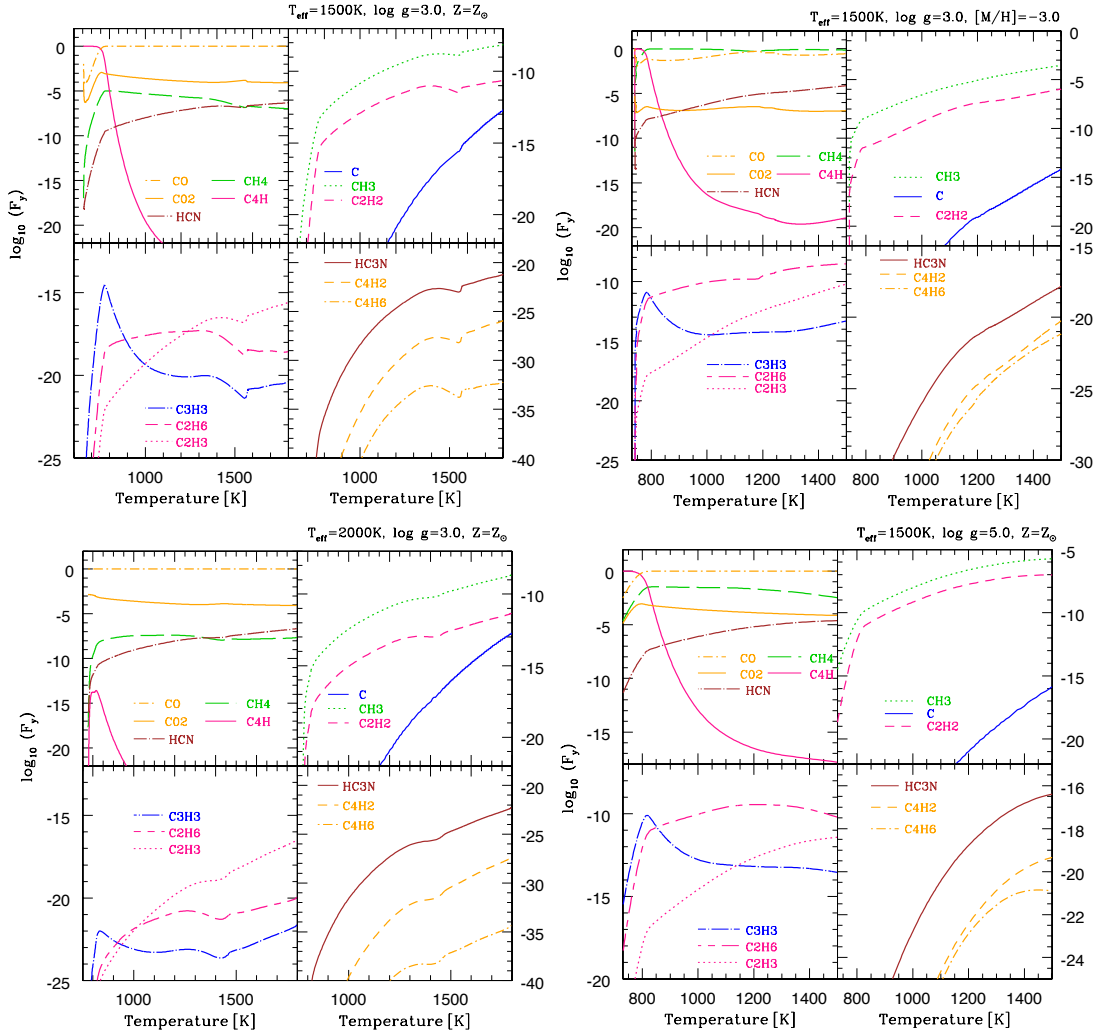


**Figure 8.** Fraction,  $F_y$ , of carbon in species  $y$  for the cloud layer of a giant gas planet atmospheric model of solar composition ( $T_{\text{eff}} = 1500\text{K}, 2000\text{K}$ ) and low-metallicity composition ( $T_{\text{eff}} = 1500\text{K}$ ) based on a DRIFT-PHOENIX. Below  $T \sim 500\text{K}$ , more carbon is bound in the hydrocarbon species  $\text{C}_4\text{H}$  than in  $\text{CO}$ .

overtaken by  $\text{CH}_4$ . This effect is more pronounced in high surface gravity objects. Due to the favourable conditions to the formation of H-bearing molecules,  $\text{C}_2\text{H}_6$  is now a more important atmospheric reservoir for carbon than  $\text{C}_2\text{H}_3$  and  $\text{C}_3\text{H}_3$  throughout the entire cloud layer.

#### 4.5 Carbon-rich substellar atmospheres

In extrapolation of our results so far, we show how the gas-phase composition would change if more carbon becomes available in an example giant gas planet atmosphere. We use the same DRIFT-PHOENIX model atmosphere structures as before ( $T_{\text{eff}}=1500\text{K}$ ,  $\log(g)=3.0$  and solar element abundances), but now we change the carbon element abundance such that more carbon than oxygen is available, hence  $\text{C}/\text{O}=1.1$  in our equilibrium chemistry routine (Figure 9). No feedback onto the radiative transfer is taken into account.

In comparison to an oxygen-rich atmosphere ( $\text{C}/\text{O} < 1$ ), the hydrocarbons and the PAHs are significantly more abundant if

$\text{C}/\text{O} > 1$  even only moderately. For example, the number densities of  $\text{CN}$  and  $\text{C}_2\text{H}_2$  have increased significantly by 5 and 10 orders of magnitude, respectively (compare Sect. 4.3).  $\text{C}_2\text{H}_2$  is now as abundant as the typical molecules encountered in oxygen-rich environments (compare Fig. 4).  $\text{C}_2\text{H}_2$  now dominates over  $\text{H}_2\text{O}$  throughout the entire atmosphere while  $\text{CH}_4$  dominates over  $\text{H}_2\text{O}$  until  $T=3000\text{K}$ . Figure 9 shows further that carbon-monoxide is the most dominant C-bearing species in the model atmosphere used for this study.  $\text{H}_2\text{O}$  and  $\text{NH}_3$  are of comparable abundance.

The importance of the larger amongst the PAHs has increased considerably by increasing the carbon such that  $\text{C}/\text{O} > 1$  (lower panel, Fig. 9 and Fig. 10).

Helling et al. (1996) predicted the formation of PAHs with large concentrations in the layers of dynamical carbon-rich stellar atmospheres when  $T \leq 850\text{K}$  (for higher effective temperature and smaller surface gravity than the models studied in the present work). In our study, the PAHs are important between a gas temperature of  $1000\text{K}$  and  $1500\text{K}$  (Fig. 9). We recovered the same molecular concentration for  $\text{C}_6\text{H}_2$ ,  $\text{C}_2\text{H}_2$  and  $\text{HCN}$  as Helling et al. (1996)

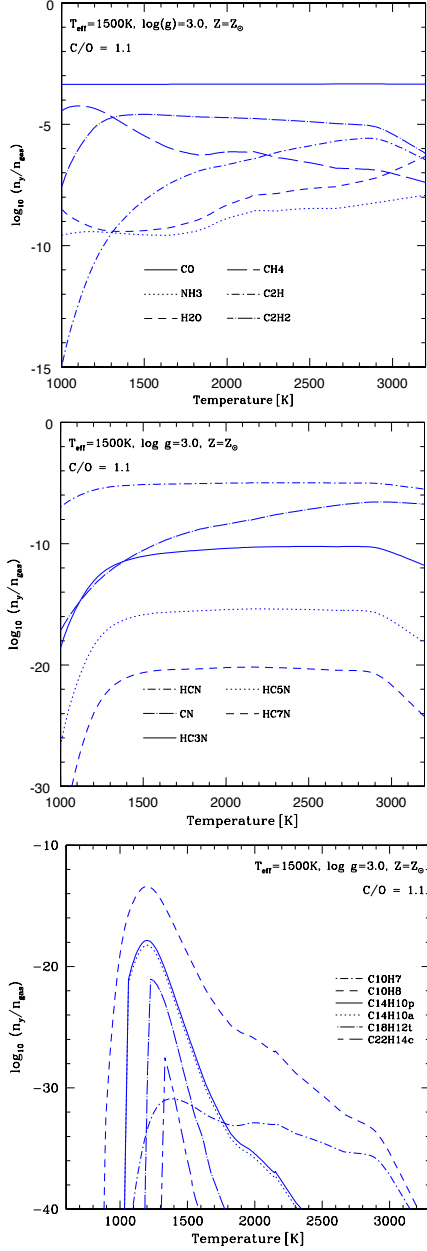


**Figure 9.** Chemical equilibrium abundances for small and large carbon-bearing molecules for a carbon-rich ( $C/O = 1.1$ ) giant gas planet based on a DRIFT-PHOENIX model atmosphere for  $T_{\text{eff}}=1500\text{K}$ ,  $\log(g)=3.0$  and solar element abundances.

throughout the atmosphere; whereas  $\text{CH}_4$  and  $\text{HC}_3\text{N}$  are higher in concentration in our model giant gas planet.

## 5 DEPARTURE FROM CHEMICAL EQUILIBRIUM BY CONVECTIVE MIXING

So far, we have studied how abundant carbon-binding macromolecules can be in local chemical equilibrium in brown dwarf and giant gas planet atmospheres. Our results suggest that  $\text{C}_2\text{H}_6$  becomes gradually more important than  $\text{C}_2\text{H}_2$  in low-metallicity

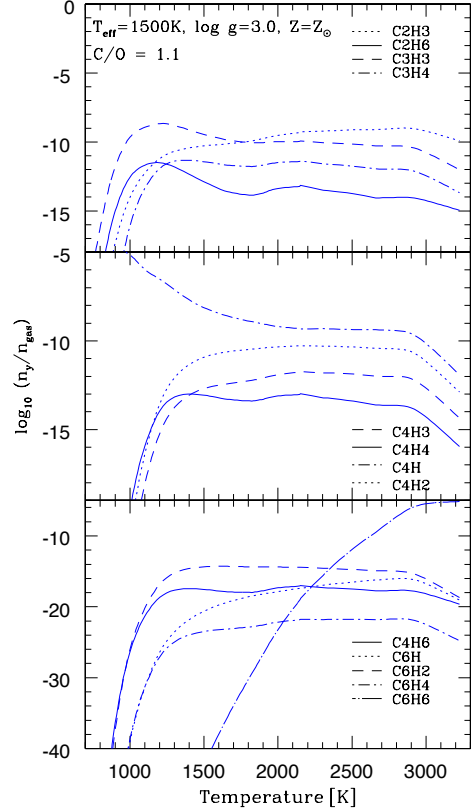


**Figure 10.** Hydrocarbon abundances for a DRIFT-PHOENIX model gas-giant atmosphere of  $T_{\text{eff}}=1500\text{K}$ ,  $\log(g)=3.0$ , solar element abundance and also artificially increased carbon-abundances, such as  $C/O=1.1$ .

atmospheres as relatively less carbon is available. We now study possible deviations from the thermochemical equilibrium values by a simple time-scale comparison.

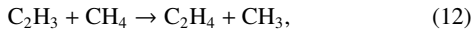
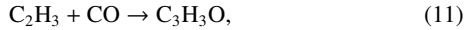
The major carbon-binding molecules in a solar metallicity gas,  $\text{CO}$  and  $\text{CH}_4$ , are rather small. Both, however, have been shown to be affected when vertical mixing processes are faster than their destruction kinetics. According to Moses et al. (2011) and Prinn & Barshay (1977) transport time scale arguments can be used to predict the abundance of  $\text{CH}_4$  at its quenching point in the atmosphere.

Next, we examine the potential influence of the transport-induced quenching on the hydrocarbon chemistry. Above the thermochemical regime in the deep atmosphere, where equilibrium is maintained via rapid reaction kinetics, a quenched regime may exist for some species, where rapid atmospheric transport and slow reaction kinetics drive constituents out of equilibrium. As a result, the abundance of molecules can be different from their equilibrium value at the same height in the atmosphere. We investigate three pre-selected hydrocarbon species,  $\text{C}_2\text{H}_2$ ,  $\text{C}_2\text{H}_6$  and  $\text{C}_2\text{H}_3$ , which among the atmospheric hydrocarbon inventory, become increasingly important in the deeper atmospheric layers.

There is good reason to think that  $\text{CO}$  and  $\text{CH}_4$  are quenched, and their quenching height may affect the dominant destruction pathway for  $\text{C}_2\text{H}_x$  species. This may happen in two ways. Either (1)  $\text{CO}$  or  $\text{CH}_4$  directly destroys  $\text{C}_2\text{H}_x$ , or (2)  $\text{CO}$  or  $\text{CH}_4$  is involved in the formation or destruction of the species that destroy  $\text{C}_2\text{H}_x$ . We are capable of applying our first-order approximation

of  $t_{\text{chem}}$  to explore (1). Considering only the direct destruction of  $\text{C}_2\text{H}_x$  is a simplification that involves profound uncertainties. The full effect of  $\text{CH}_4$  and  $\text{CO}$  cannot be accounted for under such a simplification, and these may impact the abundances of various species that destroy  $\text{C}_2\text{H}_x$  such that other destruction routes may dominate. This would be the case, however, even if  $\text{CH}_4$  and  $\text{CO}$  were not quenched; we only consider direct destruction routes for these  $\text{C}_2\text{H}_x$  species.

The reactions that destroy  $\text{C}_2\text{H}_2$ ,  $\text{C}_2\text{H}_3$  and  $\text{C}_2\text{H}_6$  that involve  $\text{CO}$  or  $\text{CH}_4$  and meet criteria (i) - (iii) in Section 3.2 are:



with rate coefficients taken from Tsang & Hampson (1986). There are no known reactions involving  $\text{C}_2\text{H}_6$  and  $\text{CO}/\text{CH}_4$ . In order to find the maximum direct effect of  $\text{CO}$  and  $\text{CH}_4$  quenching on relaxation time-scales for  $\text{C}_2\text{H}_2$ ,  $\text{C}_2\text{H}_3$  and  $\text{C}_2\text{H}_6$ , we consider the rates of these reactions with  $\text{CO}$  and  $\text{CH}_4$  quenched at the highest pressures considered in our DRIFT-PHOENIX model atmospheres. It turns out that Reactions (11),(12) are both much slower than the destruction of  $\text{C}_2\text{H}_3$  by  $\text{H}_2$ , and so the quenching of  $\text{CO}$  and  $\text{CH}_4$  does not directly affect the quenching height for  $\text{C}_2\text{H}_3$ . The relaxation time-scale  $t_{\text{chem}}$  is shorter for both destruction reactions for  $\text{C}_2\text{H}_2$  in Table 1 than for Reaction 10, even assuming the maximum possible abundance of  $\text{CO}$  due to quenching. Reaction (13) is endothermic, with a barrier of  $\sim 43000$  K, but the reverse reaction is severely impeded in the upper atmosphere by the depletion of  $\text{HCO}$ . If  $\text{CO}$  is not quenched, then the reverse reaction,  $\text{HCO} + \text{C}_2\text{H}_5$  dominates throughout the atmosphere. If, however,  $\text{CO}$  is quenched at the highest pressure we consider for our model atmospheres, then Reaction (13) dominates in the  $\log g = 3$ , solar metallicity case when  $p_{\text{gas}} \lesssim 10^{-5}$  bar. Nevertheless, the relaxation time-scale for this reaction is much larger than any of the dynamical time-scales, and so this reaction does not help to determine the quenching height of  $\text{C}_2\text{H}_6$ . The time-scale comparison for Reactions (10)-(12) are plotted in Fig. 11.

The reaction pathways studied here are approximated to be rate-determining steps, since no data could be found available with full reaction schemes of hydrocarbons in substellar environments. Each molecular interconversion, such as  $\text{CO}/\text{CH}_4$  and  $\text{N}_2/\text{NH}_3$ , are usually a full reaction scheme that consists of many reactions including the rate-determining step. The applicability of reaction schemes are also dependent on the atmospheric structure studied, and the uncertainties on the kinetic rate coefficients make the field of reaction kinetics very challenging as is clear from the wide range of time-scales for single reactions in Figs. 12,13.

For three pre-selected hydrocarbon species,  $\text{C}_2\text{H}_2$ ,  $\text{C}_2\text{H}_6$  and  $\text{C}_2\text{H}_3$ , we find the following:

$\text{C}_2\text{H}_2$ : Figure 12 compares the chemical relaxation time-scales for  $\text{C}_2\text{H}_2$  to the convective mixing time-scale and turbulent diffusion time-scale. In the solar-composition giant gas planet model, the quench level of  $\text{C}_2\text{H}_2$  can occur at atmospheric pressures as high as  $p_{\text{gas}} \approx 3 \times 10^{-3}$  bar down to  $p_{\text{gas}} \approx 10^{-5}$  bar. The intersection of  $t_{\text{mix}}$  and  $t_{\text{chem}}$  occurs at different pressures for all three models. When  $\log g = 5$  (solar metallicity), quenching occurs somewhere in the range  $10^{-3}$  bar  $< p_{\text{gas}} < 3 \times 10^{-2}$  bar. In the low metallicity

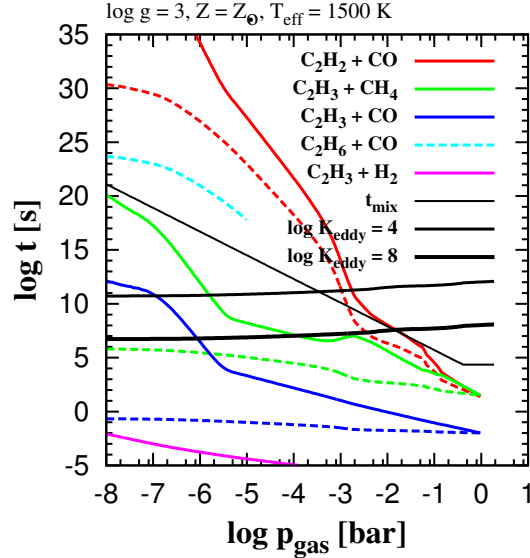
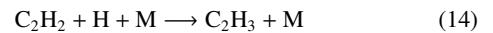


**Figure 11.** Relaxation and dynamical time-scales for our  $\log g = 3$ ,  $T_{\text{eff}} = 1500$  K, solar metallicity model atmosphere, as a function of pressure [bar]. The colored lines represent relaxation time-scales for Reactions (10, red), (11, blue), (12, green) and (13, cyan). Solid lines are the time-scales when  $\text{CO}$  and  $\text{CH}_4$  are not quenched. Dashed lines are the time-scales when  $\text{CO}$  and  $\text{CH}_4$  are quenched at  $\sim 1$  bar. The plot for Reaction (13) only extends to  $p_{\text{gas}} < 10^{-5}$  bar, because at higher pressures, the reverse reaction,  $\text{C}_5\text{H}_2 + \text{HCO}$ , dominates. The solid purple line is the relaxation time-scale for  $\text{C}_2\text{H}_3 + \text{H}_2$ .

case ( $\log g = 3$ ,  $[\text{M}/\text{H}] = -3$ ), quenching occurs within the range  $10^{-4}$  bar  $< p_{\text{gas}} < 3 \times 10^{-2}$  bar.

Transport-induced quenching has been extensively studied also by Moses et al. (2011) in the atmospheres of hot Jupiters. A dominant interconversion scheme for  $\text{C}_2\text{H}_2 \rightarrow \text{CH}_4$  is proposed (Moses et al. 2011, their Eq. 9), of which the rate-determining step



is included in Table 1, along with the combustion reaction for  $\text{C}_2\text{H}_2$ . Moses et al. (2011) found that disequilibrium chemistry enhances the abundances of acetylene ( $\text{C}_2\text{H}_2$ ) in the atmospheres of hot Jupiter exoplanets.

$\text{C}_2\text{H}_3$ : The quenching-study approach fails for species that have no quench point, i.e. no disequilibrium number density of the species can be estimated for above the quench level, only a comparison between the mixing and chemical timescales can be made. For example, the destruction of  $\text{C}_2\text{H}_3$  through reaction with molecular hydrogen is unquenchable. This can be easily determined from Fig. 11, since the relaxation time-scale for  $\text{C}_2\text{H}_3$  is orders of magnitude lower than the fastest dynamical time-scales considered for our model atmospheres. It results that vertical mixing cannot freeze out  $\text{C}_2\text{H}_3$  destruction, and one cannot use our simple approximation of the quenching kinetics in this case to draw conclusions on the disequilibrium abundance of  $\text{C}_2\text{H}_3$ .

$\text{C}_2\text{H}_6$ : Figure 13 shows our results for the quenching of  $\text{C}_2\text{H}_6$  according to our alternative method. The quench level candidates are intersection points between the eddy diffusion timescales and  $t_{\text{chem}}$  for the reaction:



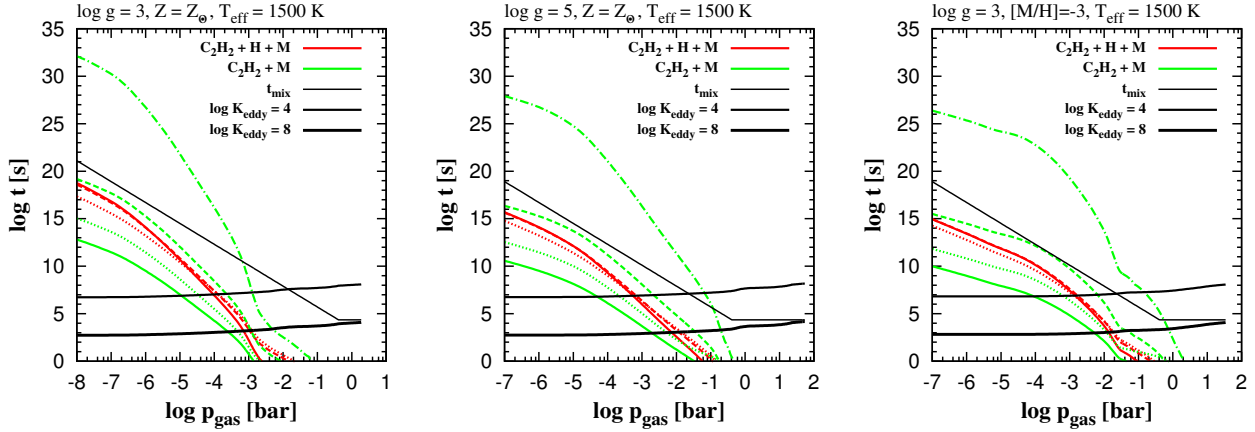


**Figure 12.** Convective mixing timescale (*thin black line*), the eddy diffusion mixing timescale (*thick black lines*) and the reaction time for the destruction  $C_2H_2$  when a) (left)  $\log g = 3$ ,  $Z = Z_\odot$ ,  $T_{\text{eff}} = 1500$  K (giant gas planet), b) (middle)  $\log g = 5$ ,  $Z = Z_\odot$ ,  $T_{\text{eff}} = 1500$  K (brown dwarf), c) (right)  $\log g = 3$ ,  $[M/H] = -3$ ,  $T_{\text{eff}} = 1500$  K (oxygen-depleted giant gas planet). The colored lines represent time-scales for various published rate coefficients. For the three-body destruction pathway, we show rate coefficients from Baulch et al. (1992, solid red, also Tsang & Hampson 1986; Hoyermann et al. 1968), Tsang & Hampson (1986, dashed red) and Benson & Haugen (1967, dotted red). For the combustion reaction, coefficients are from Durán et al. (1989, solid green, also Benson 1989), Thraen et al. (1982, dashed green), Palmer & Dormish (1964, dotted green) and Warnatz (1984, dash-dotted green, also Tsang & Hampson 1986).

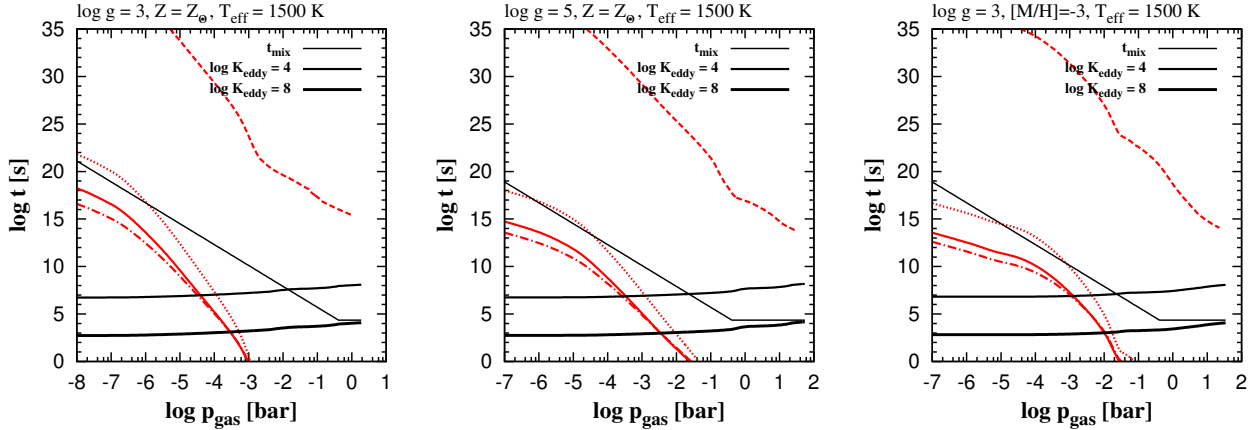


**Figure 13.** Same as Figure 12 but for  $C_2H_6$  combustion. The time-scales for various rate-coefficients are shown in red. Rate coefficients are taken from Oehlschlaeger et al. (2005, solid), Baulch et al. (1992, dashed), Izod et al. (1971, dotted) and Warnatz (1984, dash-dotted). The time-scale resulting from the theoretical rate coefficient of Kiefer et al. (2005) were also considered, but the relaxation time-scale for their rate coefficient is greater than the age of the universe over the entire pressure range.

For  $C_2H_6$ , quenching may occur at pressures as low as  $10^{-3}$  bar. By increasing the eddy diffusion, the eddy diffusivity mixing time decreases. Consequently, the intersection of  $t_{\text{mix,eddy}}$  and  $t_{\text{chem}}$  occurs at a higher range of pressures yielding a higher non-equilibrium number density of acetylene and  $C_2H_6$  over a large extent of the atmosphere (compare thick black line in Figs. 12, 13). Despite the uncertainties in the rate coefficient for Reaction 15, a lower limit to the quenching height can be established.

## 6 DISCUSSION

Our exploration of the effects that dust formation has on gas-phase metallicity and as a result on the equilibrium chemistry has yielded some surprising results. Although only affecting the C/O by bringing it from 0.5 to 0.7, dust formation results in the depletion of metals like silicon and titanium by several orders of magnitude,

and has had an orders-of-magnitude impact on the chemistry. Also remarkable is the stability of benzene in the deep atmosphere. We note particularly the high abundance of  $C_4H$  at low temperatures and the impact of various published rate coefficients on predictions for the quenching heights and time-scales, both of which we discuss below.

### 6.1 $C_4H$ abundance

Our results suggest high abundances of  $C_4H$  which is somewhat surprising as  $C_4H$  is a radical and should therefore be destroyed easily. We checked the equilibrium constants and none of them behaves strangely when plotted, nor are they used outside that tested temperature interval. We cannot find any obvious errors with our calculation with respect to any of the molecules considered here, including  $C_4H$ .

Surprisingly high abundances of  $C_4H$  have been observed in the interstellar medium (e.g. Pety et al. 2005), in cometary ice (Geiss et al. 1999), and are believed to play an important role in the complex carbon chemistry within Titan’s atmosphere (Berteloite et al. 2008). It is believed that the high amount of  $C_4H$  cannot be accounted for by gas-phase thermochemistry, but is formed as a product of PAH destruction, within the cometary ice itself, or via photodissociation (Leonori et al. 2008). It is interesting that our thermochemical equilibrium contains high amounts of  $C_4H$ , without having accounted for any of these possible sources. The condensation of heavy elements in the gas onto grains, and the impact on the metallicity, may partially explain the high abundances of  $C_4H$  observed in comets and the interstellar medium, and inferred to be present in the atmosphere of Titan.

## 6.2 Uncertainties due to differences in rate coefficient

Given the various rate networks employed in the literature, we assess the impact of the different material data on the quenching point. For this, we utilise  $C_2H_6$  quenching. The uncertainties in the rate coefficient for Reaction (15) (Table 1) span an order of magnitude or more amongst the different rate coefficient data sources. For example, two values for  $k_0$  [ $cm^3 s^{-1}$ ] for the  $C_2H_6$  combustion reaction given in Baulch et al. (1992) have identical values of  $n$  and  $E_a$ , but values of  $A = 7.5 \times 10^{-20} cm^3 s^{-1}$  and  $4.5 \times 10^4 cm^3 s^{-1}$ , a difference of about 24 orders of magnitude. A more typical disagreement would be between the  $k_0$  values for this same reaction between Baulch et al. (1992) and Warnatz (1984), which at 800 K is about an order of magnitude, although these two rate coefficients come into much better agreement at high temperatures.

Concerning the destruction of  $C_2H_2$  by the three-body interaction with hydrogen, we examined in detail published rate coefficients from reviews (Baulch et al. 1992; Tsang & Hampson 1986), experiment (Hoyerermann et al. 1968) and theory (Benson & Haugen 1967). For the combustion of  $C_2H_2$ , we examined the review of rate coefficients from Durán et al. (1989), as well as the experimentally determined rate coefficients from Thraen et al. (1982) and Palmer & Dormish (1964) and the rate coefficients determined theoretically by Benson (1989). Finally, for  $C_2H_6$  combustion into  $2CH_3$ , we considered the reviewed rates from Baulch et al. (1992); Warnatz (1984), as well as experimental (Oehlschlaeger et al. 2005; Izod et al. 1971) and theoretical calculations (Kiefer et al. 2005) of these rate coefficients. The range of values for the rate coefficients over the pressure range is incredible, and its impact on the chemical time-scales spans 15 orders of magnitude, as can be seen in Figs. 12 and 13. Three-body rate coefficients are very difficult to constrain from high temperature experiments, and theoretical work is therefore also fairly unconstrained. These large uncertainties pose a problem not only for our work, but even more so for the non-linear chemical kinetics models applied to these atmospheres. Improved experimental and theoretical determinations of these rate constants are essential to progress beyond the first order approximation employed in this paper.

This leads in the case of  $C_2H_6$  that there is no definite upper limit to the quenching pressure. Figure 13 depicts the results for the different rate coefficients in different lines styles which shows that it is possible that  $t_{chem} > t_{diff}$  for the entire range of pressures considered in the DRIFT-PHOENIX model atmospheres. The reason for this is the uncertainty of the values of the rate coefficients alone.

It will be important for future chemical kinetics modelling to more carefully explore the efficiency of Reaction (15).

In the case of  $C_2H_2$ , the termolecular destruction with atomic hydrogen has a relatively small uncertainty, and if it were the only dominant reaction for destroying  $C_2H_2$ , its quenching height would likewise be well-constrained. The rate coefficient for  $C_2H_2$  combustion is far less accurate, but it still provides a range of quenching heights; the uncertainties do not overwhelm our analysis. The fact that  $C_2H_3$  reacts with molecular hydrogen means that it should not have a quenching height at all.

We note again that the data uncertainties do also apply to full-network considerations. Every quenching height given in the literature will therefore change if the material data change. Hence, quenching heights should in general be rather given as a limit  $\pm$  uncertainty.

## 7 CONCLUSION

It must be acknowledged that small hydrocarbon molecules are able to form in an oxygen-rich environment such as the atmosphere of Brown Dwarfs and giant gas planets. These molecules do not form in very significant concentrations in comparison to carbon-rich atmospheres; nonetheless, an increased surface gravity and/or decreasing metallicity combined with a greater C/O ratio inside the dust clouds improve the chance of PAH formation. A decrease of the oxygen abundance caused by oxygen-depletion due to cloud formation does support the appearance of complex carbon-binding molecules. These results contradict the general belief that hydrocarbon equilibrium chemistry is not expected in the atmospheres of Brown Dwarfs and giant gas planets where the C/O ratio is less than unity. It must be noted that hydrocarbon chemistry in irradiated giant planets, through non-equilibrium photochemistry, is theoretically predicted and observed (Zahnle et al. 2009). The formation of hydrocarbons in hot Jupiters with temperatures below 1000K is driven by the photodissociation of methane; the products -  $C_2H_2$ ,  $C_2H_4$  and  $C_2H_6$  - further polymerise to build complex PAHs and hydrocarbon aerosols, called soots, which are thought to be involved in the prebiotic evolutionary processes towards the emergence of amino acids (Tielens 2008). For wavelengths at which the dust cloud is transparent, the deep atmospheric layers can be observed. Due to the relatively significant number densities of benzene ( $C_6H_6$ ), the vinyl radical ( $C_2H_3$ ) and acetylene ( $C_2H_2$ ) predicted in our work in this region, one might expect a signature in the absorption lines.

A recent work by Fortney (2012) discussed the possibility of the formation of carbon-rich giant planets in disks where the “condensation of solids can lead to non-stellar C/O ratios in nebula gases”, in accordance with the idea used in the present work. Furthermore, Fortney (2012) raises the question of the detection of carbon-rich Brown Dwarfs that may have been eluded so far (2MASS and SDSS) simply because the spectral appearance of a Brown Dwarf with refractory clouds that remove oxygen from the gas-phase will be different: different molecules will influence the opacities and thus, the absorption lines in the atmosphere. The present work is a step forward in determining the chemical species whose opacities may yield to spectra that appear distinctly different from objects with no oxygen-depleted refractory clouds.

An interesting process to consider would be the transport of the deeper-layer hydrocarbons upward into the cloud layer. Additionally, one could imagine hydrocarbons sticking on the surface of dust grains, producing dark soot grains. This new piece of chemistry could lower the albedo of a gas giant or a Brown Dwarf, by rendering its spectral appearance “darker”. A recent work by Tian et al. (2012) studied the formation mechanism of PAH molecules in interstellar and circumstellar environments by looking at reactions of acetylene over silicate particles like forsterite ( $\text{MgSiO}_4$ ), a particularly abundant dust particle in the clouds of brown dwarfs. Their experiments lead to the production of gas-phase PAHs such as anthracene, naphthalene, phenanthrene and pyrene.

## 8 ACKNOWLEDGEMENTS

We highlight financial support of the European Community under the FP7 by an ERC starting grant. The computer support at the School of Physics & Astronomy in St Andrews is highly acknowledged. Most literature search has been performed using ADS. Our local computer support is highly acknowledged.

## REFERENCES

- Baulch D. L., Cobos C. J., Cox R. A., Esser C., Frank P., Just T., Kerr J. A., Pilling M. J., Troe J., Walker R. W., Warnatz J., 1992, *Journal of Physical and Chemical Reference Data*, 21, 411
- Benson, S. W., & Haugen, G. R. 1967, *The Journal of Physical Chemistry*, 71, 1735
- Benson, S. W. 1989, *International Journal of Chemical Kinetics*, 21, 233
- Berteloite C., Le Picard S. D., Birza P., Gazeau M.-C., Canosa A., Bénilan Y., Sims I. R., 2008, *Icarus*, 194, 746
- Carrasco N., Plessis S., Dorbijejevic M., Pernot P. 2008, *Int. J. Chem. Kinetics* 40(11), 699
- Cherchneff I., Barker J. R., 1992, *ApJ*, 394, 703
- Dehn M., 2007, PhD thesis, Univ. Hamburg
- Durán, R. P., Amorebieta, V. T., & Colussi, A. J. 1989, *International Journal of Chemical Kinetics*, 21, 947
- Fortney, J. J., Cooper, C. S., Showman, A. P., Marley, M. S., & Freedman, R. S. 2006, *ApJ*, 652, 746
- Fortney, J. J., Shabram, M., Showman, A. P., et al. 2010, *ApJ*, 709, 1396
- Fortney J. J., 2012, *ApJ*, 747, L27
- Gaidos E. J., 2000, *Icarus*, 145, 637
- Gail H.-P., Sedlmayr E., 1986, *A&A*, 166, 225
- Geiss J., Altwegg K., Balsiger H., Graf S., 1999, *Space Sci. Rev.*, 90, 253
- Grevesse N., Asplund M., Sauval A. J., 2007, *Space Sci. Rev.*, 130, 105
- Hauschildt P.H., Baron E. 1999, *JCoAM* 109, 41
- Helling C., Ackerman A., Allard F., Dehn M., Hauschildt P., Homeier D., Lodders K., Marley M., Rietmeijer F., Tsuji T., Woitke P., 2008, *MNRAS*, 391, 1854
- Helling C., Dehn M., Woitke P., Hauschildt P. H., 2008, *ApJ*, 675, L105
- Helling C., Jorgensen U. G., Plez B., Johnson H. R., 1996, *A&A*, 315, 194
- Helling C., Woitke P., 2006, *A&A*, 455, 325
- Hoyermann, K., Gg. Wagner, H., & Wolfrum, J. 1968, *Berichte der Bunsengesellschaft für physikalische Chemie*, 72, 1004
- Izod, T. P. J., Kistiakowsky, G. B., & Matsuda, S. 1971, *J. Chem. Phys.*, 55, 4425
- Kiefer, J. H., Santhanam, S., K., S. N., et al. 2005, *Proceedings of the Combustion Institute*, 30, 1129
- Klotz H. D., Drost H., Spangenberg H. J., 1980, *Z. Phys. Chem.*, 261
- Knyazev V. D., Bencsura À., Stoliarov S. I., Slagle I. R., 1996, *Journal of Physical Chemistry*, 100, 11346
- Kopparapu, R. k., Kasting, J. F., & Zahnle, K. J. 2012, *ApJ*, 745, 77
- Leggett S. K., Saumon D., Marley M. S., Geballe T. R., Golimowski D. A., Stephens D., Fan X., 2007, *ApJ*, 655, 1079
- Leonor F., Petrucci R., Hickson K. M., Segoloni E., Balucani N., Le Picard S. D., Foggi P., Casavecchia P., 2008, *Planet. Space Sci.*, 56, 1658
- Line M. R., Liang M. C., Yung Y. L., 2010, *ApJ*, 717, 496
- Lodders K., Fegley B., 2002, *Icarus*, 155, 393
- Madhusudhan N., Harrington J., Stevenson K. B., Nymeyer S., Campo C. J., Wheatley P. J., Deming D., Blecic J., Hardy R. A., Lust N. B., Anderson D. R., Collier-Cameron A., Britt C. B. T., Bowman W. C., Hebb L., Hellier C., Maxted P., Pollacco D., West R. G., 2011, *Nature*, 469, 64
- Miller-Ricci Kempton E., Zahnle K., Fortney J.J. 2012; *ApJ* 745, 3
- Moses, J. I., Fouchet, T., Bézard, B., et al. 2005, *Journal of Geophysical Research (Planets)*, 110, 8001
- Moses J. I., Visscher C., Fortney J. J., Showman A. P., Lewis N. K., Griffith C. A., Klippenstein S. J., Shabram M., Freedman A. J., Marley M. S., Freedman R. S., 2011, *ApJ*, 737, 15
- Oehlschlaeger M. A., Davidson D. F., K. H. R., 2005, *Proceedings of the Combustion Institute*, 30, 1119
- Palmer, H. B., & Dormish, F. L. 1964, *The Journal of Physical Chemistry*, 68, 1553
- Pety J., Teyssier D., Fossé D., Gerin M., Roueff E., Abergel A., Habart E., Cernicharo J., 2005, *A&A*, 435, 885
- Prinn R. G., Barshay S. S., 1977, *Science*, 198, 1031
- Saumon D., Geballe T. R., Leggett S. K., Marley M. S., Freedman R. S., Lodders K., Fegley Jr. B., Sengupta S. K., 2000, *ApJ*, 541, 374
- Saumon D., Marley M. S., Cushing M. C., Leggett S. K., Roellig T. L., Lodders K., Freedman R. S., 2006, *ApJ*, 647, 552
- Saumon D., Marley M. S., Leggett S. K., Geballe T. R., Stephens D., Golimowski D. A., Cushing M. C., Fan X., Rayner J. T., Lodders K., Freedman R. S., 2007, *ApJ*, 656, 1136
- Seager S., Kuchner M., Hier-Majumder C. A., Militzer B., 2007, *ApJ*, 669, 1279
- Showman, A. P., Fortney, J. J., Lian, Y., et al. 2009, *ApJ*, 699, 564
- Thraen, H., Winkelmann, G., & Spangenberg, H. J. 1982, *Zeitschrift für Chemie*, 22, 222
- Tian M., Liu B. S., Hammonds M., Wang N., Sarre P. J., Cheung A. S.-C., 2012, *Phys. Chem. Chem. Phys.*, 14, 6603
- Tielens A. G. G. M., 2008, *ARA&A*, 46, 289
- Tsang W., Hampson R. F., 1986, *Journal of Physical and Chemical Reference Data*, 15, 1087
- Tsuji T. 1973, *A&A* 23, 411
- Venot O., Hébrard E., Agúndez M., Dobrijejevic M., Selsis F., Hersant F., Iro N., Bounaceur R., 2012, *ArXiv e-prints*
- Visscher C., Moses J. I., 2011, *ApJ*, 738, 72
- Wakelam, V., Selsis, F., Herbst, E., & Caselli, P. 2005, *A&A*, 444, 883
- Wakelam, V., Herbst, E., Loison, J.-C., et al. 2012, *ApJS*, 199, 21
- Warnatz J., 1984, *Rate coefficients in the C/H/O system*. Springer-

Verlag, NY

Witte S., Helling C., Hauschildt P. H., 2009, A&A, 506, 1367

Woitke P., Helling C., 2003, A&A, 399, 297

Woitke P., Helling C., 2004, A&A, 414, 335

Zahnle K., Marley M. S., Fortney J. J., 2009a, ArXiv e-prints

Zahnle K., Marley M. S., Freedman R. S., Lodders K., Fortney  
J. J., 2009b, ApJ, 701, L20